INSTITUTE OF PHYSICS PUBLISHING NANOTECHNOLOGY
Nanotechnology **17** (2006) 5474–5479 doi:10.1088/0957-4484/17/21/030

Raman scattering studies of the low-frequency vibrational modes of bacteriophage M13 in water—observation of an axial torsion mode

K T Tsen[1], Eric C Dykeman[1], Otto F Sankey[1], Shaw-Wei D Tsen[2], Nien-Tsung Lin[3] and Juliann G Kiang[4,5,6]

[1] Department of Physics and Astronomy, Arizona State University, Tempe, AZ 85287-1504, USA
[2] Department of Pathology, Johns Hopkins Medical Institutions, Baltimore, MD 21231, USA
[3] Institute of Microbiology, Immunology and Molecular Medicine, Tzu Chi University, 701, Section 3, Chung-Yang Road, Hualien 970, Taiwan
[4] Department of Cellular Injury, Walter Reed Army Institute of Research, Silver Spring, MD 20910-7500, USA
[5] Department of Medicine, Uniformed Services University of the Health Sciences, Bethesda, MD 20814-4799, USA
[6] Department of Pharmacology, Uniformed Services University of the Health Sciences, Bethesda, MD 20814-4799, USA

Received 3 September 2006, in final form 4 September 2006
Published 20 October 2006
Online at stacks.iop.org/Nano/17/5474

Abstract
Low-wavenumber ($\leqslant 20\ \mathrm{cm}^{-1}$) acoustic vibrations of the M13 phage have been studied using Raman spectroscopy. The dominant acoustic vibrational mode has been found to be at $8.5\ \mathrm{cm}^{-1}$. The experimental results are compared with theoretical calculations based on an elastic continuum model and appropriate Raman selection rules derived from a bond polarizability model. The observed Raman mode has been shown to belong to one of the Raman-active axial torsion modes of the M13 phage protein coat. It is expected that the detection and characterization of this low-frequency vibrational mode can be used for applications in nanotechnology such as for monitoring the process of virus functionalization and self-assembly.

1. Introduction

Virus particles (virions) exist in various sizes and shapes. A typical virus particle is made up of genetic material such as DNA or RNA, surrounded by a protein coating (capsid). On the one hand, viruses can cause disastrous diseases, and therefore tremendous efforts have been made to eliminate them. Babincová *et al* [1] hypothesized that ultrasound in the GHz range could be resonantly absorbed by HIV particles, leading to their destruction. There have also been experimental studies of ultrasound absorption by empty viral capsids [2, 3], which revealed an enhanced absorption in the MHz range as proteins reassemble into a capsid; however, no concrete resonance peaks could be assigned. On the other hand, the possibility of using a virus as a template for building uniform semiconductor nanostructures seems to be increasingly plausible. Among the crucial issues associated with molecular-beam epitaxy (MBE) self-assembly for applications in nanotechnology is the variation in size [4, 5]. Manufacturing of identical or nearly identical structures at nanoscale is desirable; however, it is extremely difficult to accomplish with the conventional techniques. So far, MBE-grown nanowires, nanorods and quantum dots, which are proposed as elements in future nanoelectronic circuits, come with size dispersion despite immense efforts on the control of size and shape [6, 7]. Although the method of self-assembly by employing chemically generated templates [8, 9] decreases to some extent the size dispersion of the grown structures, the results are still not satisfactory. Recently, a technique which departs radically from conventional approaches has been proposed [10–14]. This promising technique utilizes biological objects, such as

viruses, as nanotemplates for the fabrication of nanostructure elements. For example, cylindrical viruses like the tobacco mosaic virus (TMV) and M13 phage have been successfully used as biological templates in the synthesis of semiconductor and metallic nanowires [10, 13, 14]. Furthermore, genetically modified TMV and M13 viruses have been demonstrated for use in the self-assembly of nanomaterials into liquid crystals, films and fibres [11, 12]. It is therefore very likely that genetically programmed viruses will play an important role in the next generation of nanoelectronics circuits and optoelectronic devices. In order to monitor the self-assembly processes, an *in situ*, non-destructive technique is desirable. Raman spectroscopy has been demonstrated to be a non-invasive technique in material research. In the past, however, Raman spectroscopy on viruses had been emphasized only on the large wavenumber regions ($\geqslant$600 cm^{-1}) where internal virus composition, localized vibrations of multiply bonded or electron-rich groups in proteins were studied [15]. In this paper, we report the first observation of low-wavenumber ($\leqslant$20 cm^{-1}) acoustic vibrations of M13 phages by using Raman spectroscopy. The observed vibrations are compared with theoretical calculations based on an elastic continuum model and appropriate Raman selection rules derived from the bond polarizability method. The observed Raman mode has been shown to belong to one of the Raman-active axial torsion modes of its protein coat. Because of the sensitivity of its frequency upon environments, it is expected that the detection of this low-frequency vibrational mode can be used to monitor and help to control the process of virus functionalization, such as coating with different materials, attachment to quantum dots, carbon nanotubes, and forming multiple superstructures.

2. Samples and experimental technique

The M13 phage samples in water solution used in this work were prepared as follows. To propagate the M13 phage, an overnight culture of the host cell, JM101, was diluted 20-fold into 125 ml flasks containing 20 ml of LB medium. When the culture reached 0.5 of optical density at 550 nm (OD_{550}), the phage was added at a multiplicity of infection of 20 and further grown until stationary phase (approximately 12 h post-infection). Crude phage suspensions were prepared by centrifugation (10 000g, 15 min) of the culture to remove the cells and passing the supernatants through a membrane filter (0.45 μm pore size). To concentrate the phage titre, the filtrated supernatant was precipitated by 0.25 M NaCl and 2.5% polyethylene glycol 6000 for 4 h on ice. The pellet collected by centrifugation (13 500g for 15 min at 4 °C) was dissolved in 100 μl of distilled water. To determine the phage titre, a double-layer bioassay [16] was performed on an LB agar plate.

To prevent heating of the samples by laser irradiation during the Raman scattering experiments, the second harmonic output of a cw mode-locked YAG laser was used as an excitation source [17]. The laser, which has photon energy of 2.34 eV, was operated at a repetition rate of 76 MHz and has a pulse width of about 70 ps. 90°-scattering geometry was employed. The Raman scattered signal was collected and analysed by a standard computer-controlled Raman system which included a double spectrometer and a photomultiplier tube with associated photon counting electronics. The spectrometer had a spectral resolution of about 1.0 cm^{-1}. All the data reported here were taken at $T = 300$ K.

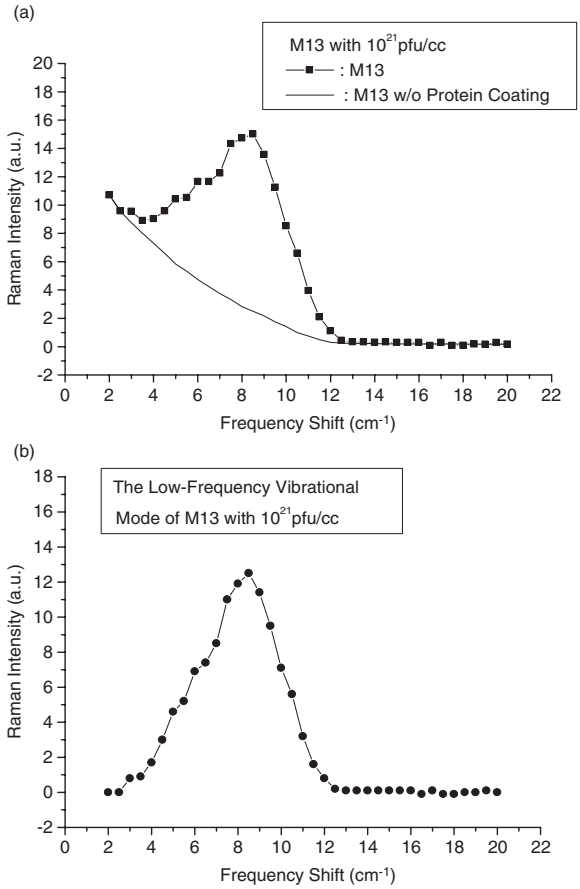

Figure 1. Raman scattering spectrum of M13 phages in water for a concentration of 10^{21} pfu ml^{-1} (a) with (solid circles) and without (solid curve) protein coat. The solid curve corresponds to the background signal due to the imperfection of rejection of elastic scattering of light by the spectrometer; (b) the low-frequency vibrational mode of M13 with a concentration of 10^{21} pfu ml^{-1} obtained after the subtraction of the background signal.

3. Experimental results and discussions

A typical Raman scattering spectrum taken for M13 phages at 10^{21} pfu ml^{-1} and in the spectral range between 2 and 20 cm^{-1} is shown in figure 1(a) (the solid circles). The distinctive feature of the spectrum is a broad structure around 8.5 cm^{-1} sitting on top of a background. To rule out both instrumental artefacts and the possibility of contributions from the DNA within the phages, we repeated the experiments with M13 phages without protein coats, i.e. with only the single-stranded M13 phage DNA at the same concentration in water solution. The results are shown as a solid line in figure 1(a). Comparison of the two spectra shows that there is indeed a broad peak at 8.5 cm^{-1} associated with scattering of light from the M13 phage protein coats. The remaining background is due to imperfections in the rejection of elastic light by the spectrometer. The actual low-frequency acoustic vibrational mode signal from the phages is obtained by the subtraction of these two spectra. Figure 1(b) shows the resulting structure

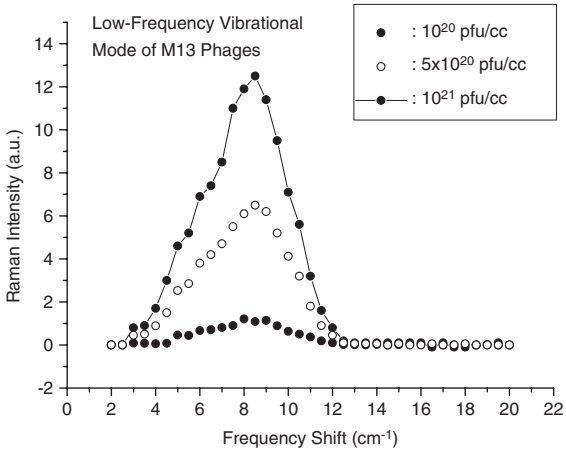

Figure 2. Raman spectra of low-frequency vibrational mode of M13 phages for three concentrations: 1×10^{20} pfu ml^{-1}, 5×10^{20} pfu ml^{-1} and 1×10^{21} pfu ml^{-1}, respectively. The Raman intensity has been found to scale with the concentration of the phages, as expected.

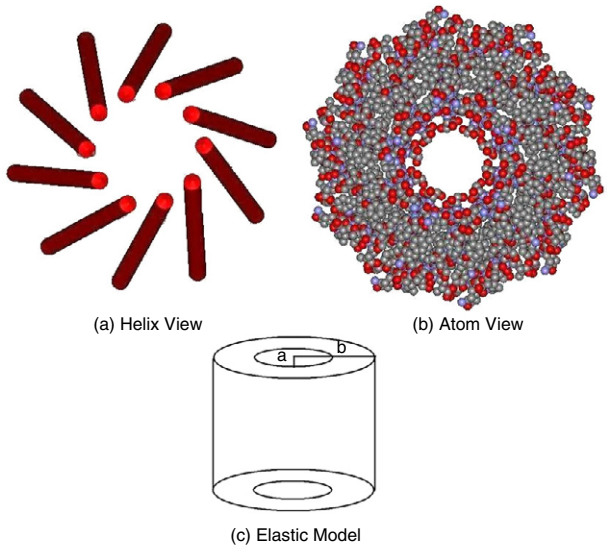

Figure 3. Diagrams of the structure of M13 phage. (a) A molecular model containing ten α-helix coat proteins forming a cone of the structure. (b) A cross section of the phage composed of α-helix coat proteins. (c) The elastic continuum model of M13; a circular cylinder of outer radius b and inner radius a.
(This figure is in colour only in the electronic version)

after the subtraction. The broad peak has been found to centre around 8.5 cm^{-1}. It has a full-width at half-maximum (FWHM) of about 5.0 cm^{-1}. Since the spectral resolution of our Raman system is about 1.0 cm^{-1}, we conclude that the relatively broad Raman peak observed here very likely results from inhomogeneous broadening.

Figure 2 shows a comparison of the observed Raman peaks for three concentrations studied: 1×10^{20}, 5×10^{20} and 1×10^{21} pfu ml^{-1}, respectively. The data are properly normalized and therefore are ready for comparison. We find that the integrated areas under the peaks scale very well with the concentration of M13 phages, as expected.

To obtain better insight into the character of the observed low-frequency vibrational Raman mode of M13 phages, we have performed theoretical calculations in which an elastic continuum model for the M13 viruses is assumed, and appropriate Raman selection rules were derived based on a continuum extension of the bond polarizability model.

4. Theoretical model calculations

Experimental Raman spectroscopy is able to observe a low-frequency mode of a cylindrical type viral particle; however, it is unable to provide a qualitative picture of the type of atomic displacements involved in the vibration. To understand what types of modes are being excited by the Raman spectroscopy experiment, we turn to a theoretical analysis of the problem.

There are several routes that can be followed in developing a theory capable of predicting Raman spectral lines, including atomistic models which give full atomic detail, to a continuum model which averages over the local geometry on the atomic scale and expands its vision to a larger length scale. The low-frequency modes being probed here through Raman scattering have long wavelengths and thus are not sensitive to atomic details. Rather they are the result of the average global properties of the phage. Our goal here is to provide qualitative insights and a semi-quantitative understanding concerning the types of vibrational modes accessible through Raman scattering of a cylindrical phage. Thus a continuum approach, when used cautiously, is a method of choice due to its relative simplicity and ease of interpretation.

In building a continuum model, it is important to first understand the structure of the M13 bacteriophage. M13 is composed of individual coat proteins bundled together so that in cross section the bundle has approximately the shape of a long circular cylinder (>860 nm), or tube [18]. Each individual coat protein in the bundle is comprised of 50 amino acids and has the conformation of an α-helix roughly aligned with the tube axis. Figure 3 shows a small segment of the filament. In cross section, there are ten individual proteins packed together. The coat proteins are packed in a partially helical fashion so that they form the shape of a cone. The narrow neck at the top of one cone fits inside the large base of the cone above it. One end of each cone contains acidic residues while the other end is basic. This produces strong cone–cone interactions which increase the stability of the assembly. The central region of the cone is apolar and enhances the interactions between α-helices of a single cone. The stacking of thousands of such cones gives the phage its long worm-like structure. Inside the core of the tube resides the ssDNA and water.

We model the long fibre as a solid cylindrical tube of elastic continuous material, as shown in figure 3(c). Following Balandin *et al* [19] the viral protein coat has an inner radius a and outer radius b. The inner and outer radii of the M13 shell are set to $a = 1.9$ nm and $b = 3.4$ nm, respectively, which were determined from the atomistic structure of the capsid by averaging over distances between atoms in the structure. Elastic wave theory [20, 21] is used to arrive at an analytic expression that describes the frequencies and displacement patterns of each vibrational mode of the cylindrical shell. Cylindrical coordinates (r, θ, z) are used, where z is the direction along the axis of the cylinder. In general, the vibrational modes depend on the wavevector k_Z varying as $e^{ik_z Z}$. We assume that the viral particle is longer than

the wavelength of the light; Raman scattering is then only produced by waves with $k_z \approx 0$. The displacement vectors of the vibrational modes are then $\vec{\vec{u}}(r, \theta)$ with no z dependence ($e^{ik_z Z} = 1$), and with components u_r (radial direction), u_θ (angular direction) and u_Z (axial direction). The radial dependence is a linear combination of Bessel functions of the first and second kinds, and the angular dependence is sinusoidal, being proportional to $\sin(n\theta)$ and $\cos(n\theta)$, where n is an integer, $n = [0, \infty]$. Since the net radial force is zero on the surfaces of the shell, the radial stress components σ_{rr}, $\sigma_{r\theta}$, and σ_{rz} must vanish at the inner and outer radii a and b. This gives six conditions relating the amplitudes that produce a 6×6 determinant [20] which must vanish at the allowed frequencies ω. There are just two parameters in the theory, and they are the longitudinal and transverse sound speeds, c_l and c_t. We use $c_l = 1817\ \mathrm{m\,s^{-1}}$ and $c_t = 915\ \mathrm{m\,s^{-1}}$, the measured sound speeds in lysozymes [22], which is similar to the measured speeds of sound in different protein crystals such as ribonuclease and haemoglobin.

Elastic wave theory provides a complete description of the possible frequencies and their displacement patterns of vibrational modes which are then used to determine their Raman scattering intensity. The Raman intensity is proportional to the Raman tensor $\Delta\chi$ as [23]

$$I \propto |\hat{d}_s \cdot (\Delta\vec{\vec{\chi}}) \cdot \hat{d}_i|^2 \tag{1}$$

where $\hat{d}_i$, $\hat{d}_s$ describe the polarization of the incident and scattered light. The Raman tensor $\Delta\vec{\vec{\chi}}$ depends on how the polarizability (due to the electromagnetic field of the laser) of the material changes with displacements produced by the vibrational mode.

For the computation of the Raman tensor we generalize the bond polarizability model [24] to a continuum-like model. We assume that the material is composed of bonds between atoms in which each bond has a derivative of the polarizability tensor with components parallel to the bond direction ($\alpha'_\parallel$) and perpendicular ($\alpha'_\perp$) due to changes in bond length. Each bond is assumed to occupy a volume V_b, and all bonds are assumed to have the same polarizability derivates. The bonds are then averaged over all random orientations. The spirit of the model is to produce a long-lengthscale theory that averages over many atoms but is derived from a tested atomistic model. The derived change of the polarizability tensor due to the strain field is

$$\Delta\vec{\vec{\alpha}} = \frac{\alpha_s}{V_b}\left(\vec{\vec{U}} - \frac{1}{3}\vec{\vec{I}} \cdot \mathrm{Tr}(\vec{\vec{U}})\right) + \frac{\alpha_c}{V_b}\mathrm{Tr}(\vec{\vec{U}})\vec{\vec{I}}. \tag{2}$$

The parameters α_s and α_c are the polarizability changes of the material due to shear strain and compressional strain, respectively. The parameters α_s and α_c are related to $\alpha'_\parallel$ and $\alpha'_\perp$, but we treat them as parameters. Our calculation only predicts relative (not absolute) intensities, so only the ratio α_c/α_s is important. We set this ratio to 1/2, which models carbon–carbon bonds well. Only the $n = 0$ modes depend on this ratio (see equations (3*a*)–(3*c*)). Details of the model are described in [25]. Integrating equation (2) over the volume of the cylindrical viral shell gives the total susceptibly tensor of the viral coat. Since the polarizability per unit volume, equation (2), is dependant on either $\cos(n\theta)$ or $\sin(n\theta)$, the integral over the angular dependence implies that the total susceptibility tensor in Cartesian coordinates is non-zero for only $n = 0$, 1 and 2 modes of the cylindrical shell. The results are

$$I \propto (2\lambda + \mu)\left[\frac{1}{3} + 2\frac{\alpha_c}{\alpha_s}\right]^2 \Gamma_0^2, \qquad \text{for } n = 0; \tag{3a}$$

$$I \propto \mu \cdot \Gamma_1^2, \qquad \text{for } n = 1; \tag{3b}$$

$$I \propto (2\lambda + \mu)\frac{\Gamma_2^2}{4}, \qquad \text{for } n = 2. \tag{3c}$$

Here λ and μ are functions of the scattering angle θ, $\lambda = [4 - 6\sin^2(\theta)]$ $\mu = [14 - \sin^2(\theta)]$, and Γ_n are numerically evaluated integrals over the displacement pattern of the modes. The experiments were performed at a scattering angle of 90°. The Γ integrals are over the displacement pattern of the vibration. For example, the $n = 0$ integral is $\Gamma_0 = \int_a^b \frac{\omega^2}{c_l^2} r\, dr[AJ_n(\omega r/c_l) + BY_n(\omega r/c_l)]$, where J_n and Y_n are Bessel functions.

Applying this theoretical foundation to the M13 bacteriophage, we find several peaks in the range of frequency range 0–25 $\mathrm{cm^{-1}}$. Figure 4 shows the modes and their Raman intensities (Gaussians broadened by 1 $\mathrm{cm^{-1}}$). Figure 4(a) shows the radial modes, figure 4(b) shows the axial modes, and all modes are shown together in figure 4(c). It is important to separate the modes by their character because the damping of the two types of mode is expected to be quite different. The radial modes will be highly damped since the atomic displacements of the virus move in or out radially, either pushing against the water on the exterior or against the water/DNA solution in the interior cavity of the virus. Axial modes produce displacements of the atoms that are parallel to the axis of the virus and hence should not interact strongly with water. The motion relative to water of the axial modes will be shear motion (rather than compressional as for radial modes) and damping will be marginal. The modes marked with a star (∗) in figure 4(c) are axial. We hypothesize that only the axial modes (those with a star) are observable in the Raman experiment because the other (radial) modes are strongly damped.

There are two main Raman intensities predicted in figure 4(c)—one at 10.5 $\mathrm{cm^{-1}}$ that is axial, and one at 20.4 $\mathrm{cm^{-1}}$ that is radial. The mode patterns of these two modes are shown in figures 5(a) and (b). The first main peak at 10.5 $\mathrm{cm^{-1}}$ is the largest, and corresponds to an $n = 1$ axial mode of vibration for the cylindrical shell. In this mode each α-helix that comprises the protein coat undergoes axial shearing. Circling about the virus by an angle θ produces a modulation of the displacement by $\cos(\theta)$ (or $\sin(\theta)$, as it is doubly degenerate). The mode pattern for one plane of atoms in a plane of the virus is similar to that of a drumhead. The second major peak at 20.4 $\mathrm{cm^{-1}}$ corresponds to radial compression/expansion of the virus. The mode has $n = 0$, so there is no dependence on the angle θ.

Our prediction for the observed Raman scattering profile is shown in figure 6. In this figure we have only included the axial modes since they should resonate with little damping. We have included a Gaussian broadening of 5 $\mathrm{cm^{-1}}$, consistent with inhomogeneous broadening observed in the experiment. The low-frequency vibrational mode observed in our Raman measurements (∼8.5 $\mathrm{cm^{-1}}$) agrees remarkably well with the

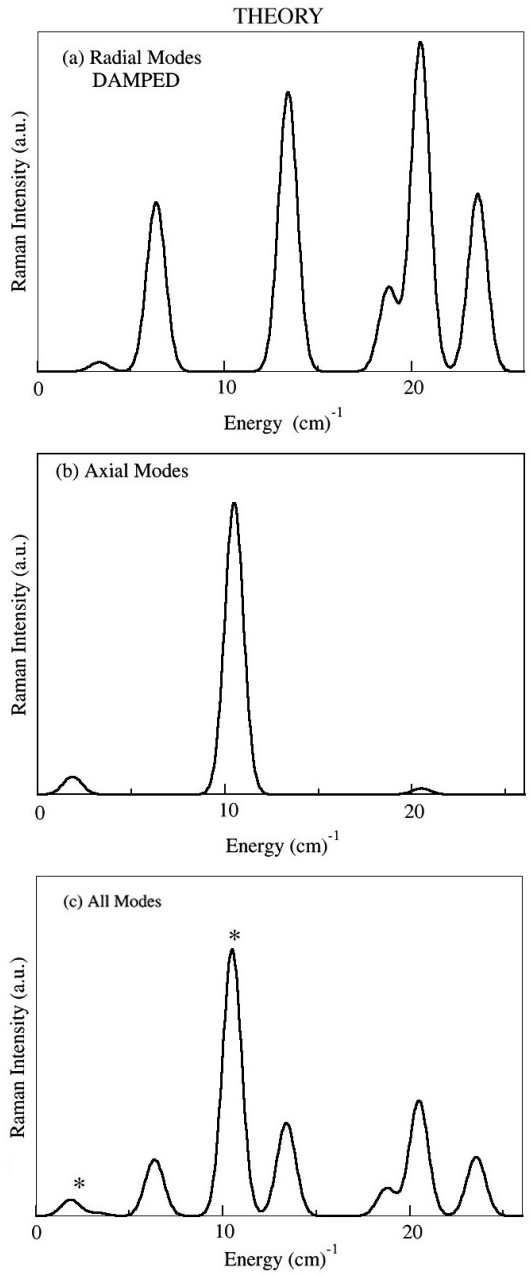

Figure 4. Theoretical Raman intensity of (a) radial modes; (b) axial modes; (c) all modes. Radial modes are expected to be highly damped by the solution. In (c), the undamped axial modes are indicated by a star (∗).

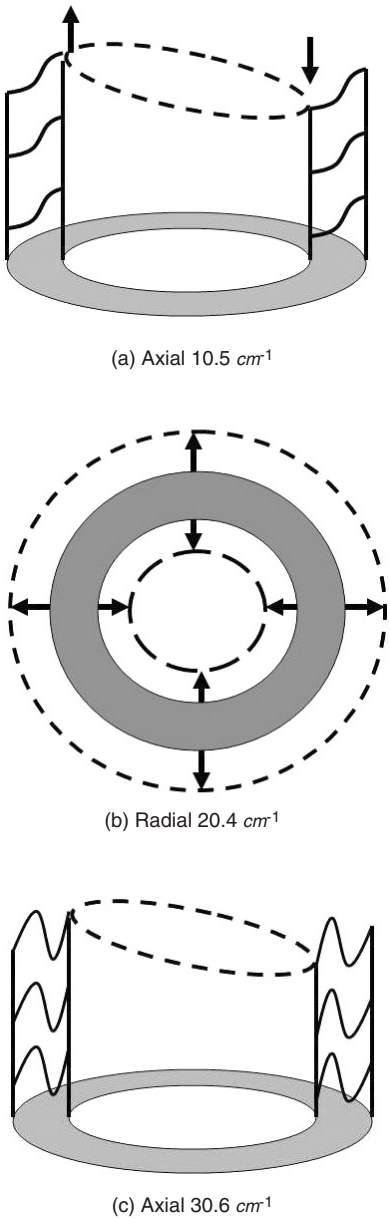

Figure 5. Cross-sectional displacement patterns for three low-frequency modes with significant Raman intensity. (a) An axial mode at 10.5 cm^{-1}. We identify this mode as the 8.5 cm^{-1} mode observed in experiment. (b) A radial mode at 20.4 cm^{-1}, expected to be damped by solution. (c) An axial mode at 30.6 cm^{-1}.

theoretical prediction of a single peak (∼10.5 cm^{-1}) produced by an axial mode.

There are many other modes of higher frequency that are predicted by the continuum model. We do not investigate frequencies higher than 25 cm^{-1} here because either (i) these modes correspond to $n > 2$ and hence are not active in Raman spectroscopy, or (ii) the modes have internal wavelengths of a few angstroms, which means that they will not be predicted reliably in a continuum model. An example of such a mode is shown in figure 5(c). This mode is just over 30 cm^{-1} and has an internal wavelength of about 10 Å. A continuum model averages over many atoms (distances of several bond lengths) and this mode is not expected to be computed accurately. Future work will develop the model further to include atomistic details and coupling of the modes with the solvent. Such extensions will further test the limits of the continuum theory, and probe deeper into our hypothesis concerning the relative importance of damping of the various modes.

In summary, the theory has identified the low-frequency modes of vibration of the M13 phage in solution and qualitatively and semi-quantitatively reproduced the observed Raman spectrum. This indicates that Raman spectroscopy is a useful, non-destructive technique for probing the low-frequency modes of the virus. These modes are global, being affected by the overall conformational properties of the virus,

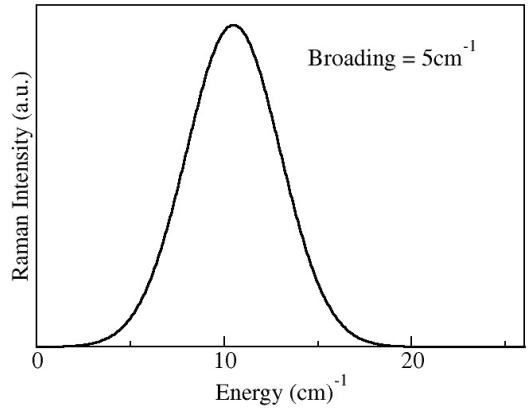

Figure 6. Final theoretical Raman intensity prediction after considering the damping effects of the solvent and the validity of the elastic continuum model.

and will be useful in providing information on how viruses are functionalized for applications in nanotechnology.

5. Conclusion

The low-frequency vibrational modes of the M13 phage have been studied by Raman spectroscopy. The primary vibrational mode has been found to be at 8.5 cm^{-1}, and its Raman intensity scales linearly with the concentration of M13 phages. The observed vibrational mode agrees well with theoretical model calculations that are based on an elastic continuum model and a bond polarizability model with Raman selection rules. With the help of theoretical data, we have determined that the observed Raman mode corresponds to an axial (drum-head-like) vibrational mode of the M13 phage protein coat which suffers minimal damping in the exterior solvent. Our results suggest that Raman spectroscopy is a feasible, non-destructive technique for probing the process of virus functionalization, such as when coating viruses with different materials, attaching viruses to quantum dots and carbon nanotubes, and forming multiple superstructures. Bacteriophage M13 is one of the simplest paradigms for viral capsids, and the characterization of its low-frequency vibrational modes is a significant step towards the use of these modes for functionalization studies on applications in nanotechnology or medical therapeutics.

Acknowledgments

This work is supported in part by the National Science Foundation under Grant No. DMR-0305147 and by DOD RAD II STO C. The opinions or assertions contained herein are the private views of the authors and are not to be construed as official or reflecting the views of the US Department of the Army, the Uniformed Services University of the Health Sciences, or the US Department of Defense.

References

[1] Babincová M, Sourivong P and Babinet P 2000 Resonant absorption of ultrasound energy as a method of HIV destruction *Med. Hypotheses* **55** 450
[2] Cerf R, Michels B, Schulz J A, Witz J, Pfeiffer P and Hirth L 1979 Ultrasonic absorption evidence of structural fluctuations in viral capsids *Proc. Natl Acad. Sci. USA* **76** 1780
[3] Michels B, Dormoy Y, Cerf R and Schulz J A 1985 Ultrasonic absorption in tobacco mosaic virus and its protein aggregates *J. Mol. Biol.* **181** 103
[4] Liu J L, Wu W G, Balandin A, Jin G and Wang K L 1999 Intersubband absorption in boron-doped multiple Ge quantum dots *Appl. Phys. Lett.* **74** 185
[5] Liu J L, Wu W G, Balandin A, Lin G, Luo Y H, Thomas S G, Lu Y and Wang K L 1999 Observation of inter-sub-level transitions in modulation-doped Ge quantum dots *Appl. Phys. Lett.* **75** 1745
[6] Kamins T I and Williams R S 1997 Lithographic positioning of self-assembled Ge islands on Si(001) *Appl. Phys. Lett.* **71** 1201
[7] Balandin A, Jin G and Wang K L 2000 Issues of practical realization of a quantum dot register for quantum computing *J. Electron. Mater.* **29** 549
[8] Bandyopadhyay S, Miller A E, Chang H C, Banerjee G, Yue D E, Ricker R E, Jones S, Eastman J A and Chandrasekhar M 1996 Electrochemically assembled quasi-periodic quantum dot arrays *Nanotechnology* **7** 360
[9] Balandin A, Wang K L, Kouklin N and Bandyopadhyay S 2000 Raman spectroscopy of electrochemically self-assembled CdS quantum dots *Appl. Phys. Lett.* **76** 137
[10] Shenton W, Douglas T, Young M, Stubbs G and Mann S 1999 Inorganic–organic nanotube composites from template mineralization of tobacco mosaic virus *Adv. Mater.* **11** 253
[11] Flynn C E, Lee S W, Peelle B R and Belcher A M 2003 Viruses as vehicles for growth, organization and assembly of materials *Acta Mater.* **51** 5867
[12] Mao C, Solis D J, Reiss B D, Kottmann S D, Sweeney R Y, Hayhurst A, Georgiou G, Iverson B and Belcher A M 2004 Virus-based toolkit for the directed synthesis of magnetic and semiconducting nanowires *Science* **303** 213
[13] Knez M, Bittner A M, Boes F, Wege C, Jeske H, Maiss E and Kern K 2003 Biotemplate of 3 nm nickel and cobalt nanowires *Nano Lett.* **3** 1079
[14] Knez M, Sumser M, Bittner A M, Wege C, Jeske H, Martin T P and Kern K 2004 Spatially selective nucleation of metal clusters on the tobacco mosaic viruses *Adv. Funct. Mater.* **14** 116
[15] Tuma R and Thomas G J 2002 Raman spectroscopy of viruses *Handbook of Vibrational Spectroscopy* ed J M Chalmers and P R Griffiths (Chichester: Wiley)
[16] Eisenstark A 1967 Bacteriophage techniques *Methods in Virology* vol 1, ed K Maramorosch and H Koprowski (New York: Academic) pp 449–524
[17] Tsen K T, Wald K R, Tobias R, Yu P Y and Morkoc H 1991 Electron–optical phonon interactions in ultrathin GaAs–AlAs multiple quantum well structures *Phys. Rev. Lett.* **67** 2557
[18] Marvin D A, Welsh L C, Symmons M F, Scott W R P and Strauss S K 2006 Molecular structure and fd (f1, M13) filamentous bacteriophage refined with respect to x-ray fibre diffraction and solid-state NMR data supports specific models of phage assembly at the bacterial membrane *J. Mol. Biol.* **355** 294–309
[19] Balandin A A and Fonoberov V A 2005 Vibrational modes of nano-template viruses *J. Biomed. Nanotechnol.* **1** 90–5
[20] Graff K F 1991 *Wave Motion in Elastic Solids* (New York: Ohio State University Press)
[21] Landau L D and Lifshitz E M 1986 *Theory of Elasticity* 3rd edn (London: Pergamon)
[22] Tachibana M, Kojima K, Ikuyama R, Kobayashi Y and Ataka M 2000 Sound velocity and dynamic elastic constants of lysozyme single crystals *Chem. Phys. Lett.* **332** 259
[23] Yu P and Cardona M 1999 *Fundamentals of Semiconductors–Physics and Materials Properties* 2nd edn (Berlin: Springer) pp 362–71
[24] Go S, Bilz H and Cardona M 1975 Bond charge, bond polarizability, and phonon spectra in semiconductors *Phys. Rev. Lett.* **34** 580–3
[25] Dykeman E C, Tsen K T and Sankey O F 2006 in preparation